PERGAMON

Mechatronics 10 (2000) 499–530

MECHATRONICS

Bio-mimetic actuators: polymeric Pseudo Muscular Actuators and pneumatic Muscle Actuators for biological emulation

Darwin G. Caldwell*, N. Tsagarakis, G.A. Medrano-Cerda

Department of Electronic Engineering, University of Salford, Salford, Lancashire, M5 4WT, UK

Abstract

Actuators, the prime drive unit in any system (biological or mechanical), are responsible for transferring energy in its many forms into mechanical motion that permits interaction with the external environment. The complexity of the organic mechanism has traditionally precluded its emulation, but a demand in robotic and other mechatronic systems for closer human interaction involving safety, redundancy, self-repair and affinity, has highlighted the potential benefits of softness, both in terms of functional and physical behaviour. This is prompting a shift in the traditional design paradigm based on motors–gears–bearings–links to a novel bio-mimetic schema based on muscle–tendon–joint–bone. Among the most fundamental features of actuators designed around this format will be a desire to emulate the performance of natural muscle in forming a safe and natural interaction medium, while still possessing the beneficial attributes of conventional engineering actuators, i.e. high power to weight/volume, high force weight/volume and good positional and force control. In this paper a study has been undertaken of two novel forms of actuators (polymeric and pneumatic Muscle), that have characteristics that can be broadly classified as giving them a range of bio-mimetic functions.

The work considers the production, modelling and performance testing of these two forms of bio-mimetic actuators. Enhancements to the performance of both systems are explored to show their capacity for bio-emulation. For the pneumatic Muscle Actuator a practical example is briefly explored to show the potential for real world applications of this technology. Finally a comparison of the relative merits of the 'muscles' are made with references to required enhancements, improvements or developments needed for viable future exploitation.

* Corresponding author.

0957-4158/00/$ - see front matter
PII: S0957-4158(99)00071-9

1. Introduction

Actuators, the prime drive unit in any system (biological or mechanical), are responsible for transferring energy in its many forms into mechanical motion that permits interaction with the external environment. This ability to interact with the surrounds is a key developmental feature of all systems [1].

Traditionally human mechanical design has employed a number of key actuation technologies that have been widely and effectively used in a variety of application domains. These include [2,3]:

1. External and later internal combustion systems that convert chemical energy through a thermal cycle into motion have formed the dominant mechanism for transport. These chemical combustion processes have spawned other systems such as rocket engines, jet engines and gas turbines, but in each instance there is a fundamental energy transfer from chemical through thermal to mechanical energy.
2. Hydraulic power in the form of cylinders has also had great success, particularly when combined with an internal combustion system that can generate the hydraulic power. This has been used to good effect in external operational environments, e.g. agriculture, construction and forestry, where great advantage can be made of the exceptionally high power and force to weight outputs. Unfortunately, oil leaks and noise have prevented widespread acceptance in indoor operations.
3. Pneumatic power with its simplified and cleaner version of hydraulic operation has found success in many industrial applications where there is a need for low cost, low precision but high power operation. The widespread use of this technology has been hampered by the lack of accurate control, but pneumatics is widely used for simple control motions and in power tools.
4. Electric motor technology through the development of electronics has found enormous applications in all motion operations and is a particular favourite in industrial applications due to its ease of use, cleanliness, low noise, good control and wide range of models. Unfortunately when mains electric supplies are not readily available the base energy storage in the form of batteries is limited and this has prevented extensive use out of doors. Nevertheless the tremendous potential has been exploited through a variety of electrical machines such as the dc motor series encompassing shunt, compound, permanent magnet, brushless and stepper designs and an equally diverse range of ac devices which have become particularly popular due to their low maintenance requirements.

That each of these systems has a domain in which they have become pre-eminent is testament to their effective operation but the fact that there are a range of actuation systems for different applications shows the difficulty or impossibility of developing an actuator for universal operation in all environments.

As the areas for technical exploitation have burgeoned and new demands are placed on the presently available actuation systems it has become increasingly

clear that these traditional systems have some significant performance limitations. These constraints are seldom more clearly demonstrated than in the area of robotics with its requirement for actuation systems to power conventional industrial devices, mini, micro and nano robots, mobile robots and to operate in environments as diverse as irradiated sites, space, sub sea, tundra or the home. With these demands and the generic requirements of mechatronic systems in mind a wide range of novel actuation systems have been developed including:

1. Variants of pneumatically driven actuators: [2,4–6] to improve the control of pneumatic cylinder based systems.
2. Piezoelectric actuators [7,8].
3. Shape memory effect actuators [9,10].
4. New hydraulic liquids based on electro-rheological fluids [11].
5. Polymeric actuators [12,13].

Consideration of these many and diverse range of man-made techniques and mechanisms for actuation shows that the natural world appears to have developed a much more ubiquitous design, with organic muscle providing power for animals ranging from the largest whales to microbes with adaptation to cope with environmental extremes. This universality in the drive process has suggested that their may be some advantages in considering at least on a macroscopic scale the biological process and trying to emulate some of the functionality.

With reference to this bio-mimetic process it can be noted that a feature of many of the new actuation systems and of robotic technology in general is a change in design emphasis, with a general evolution of design principles from the usual schema of motors–gears–bearings–links to a novel bio-mimetic mechanism of muscle–tendon–joint–bone [1]. This paradigm shift involves materials and mechanisms that will be integrated following biologically inspired operational, and regeneration patterns. Specifically the need for close interaction of these 'machines' with humans will emphasize the need for safety, redundancy, self-repair and affinity, and the benefit of softness, both in terms of functional and physical softness. Among the most fundamental features of this change of perspective will be the need for new actuation systems which can emulate the performance of natural muscle in forming a safe and natural interaction medium, while still possessing the beneficial attributes of conventional engineering actuators, i.e. high power to weight/volume, high force weight/volume and good positional and force control.

Unfortunately natural muscle has a structure in the mechanism of the muscle fibrils which cannot be replicated by technology, but on a macroscopic scale it may be possible to replicate the inherent functionality. Two actuators have particularly been identified as having potentially beneficial characteristics. These are polymeric Pseudo-Muscular Actuators based on direct mechano-chemical interactions and pneumatic Muscle Actuators (pMA).

This paper considers the production, modelling and performance testing of these two forms of bio-mimetic actuators. Enhancements to the performance of each system are explored to show their capacity for bio-emulation. For the

pneumatic Muscle Actuator a practical example is briefly explored to show the potential for real world applications of this technology. Finally a comparison of the relative merits of the 'muscles' is made with references to required enhancement, improvement or developments needed for feasible future exploitation.

2. Bio-mimetic actuators

2.1. Polymeric actuators

Polymeric materials, i.e. materials formed from smaller simpler units which are called monomers, are very widespread in nature and have been used by humans (in the form of wood and some textiles) since the earliest of times. However, it is only recently that science has produced synthetic materials with properties that can start to emulate the natural source.

Amongst polymers, gels form a particularly interesting polymeric substance that consists of a tangled network of polymer chains immersed in a liquid medium. This is the basis of muscle proteins observed in all living creatures, where the fibres are immersed in a liquid (blood or plasma), which provides nutrients and minerals sustaining their functionality. This clear biological analogy emphasizes the potential of polymeric systems.

The first artificial (long chain polymer) muscles were discovered independently by Kuhn and Katchalsky [13,14] in the late 40 s. Dilation and contraction in these materials was produced by reversible ionisation of the constituent polyionic side-chains when stimulated by acids and alkalis. Since the response was produced by variation of the pH, this muscle replicating system became known as a 'pH muscle'.

Since then the number of polymers and stimulation techniques has grown and now ranges from those that use pH and reduction-oxidation as the stimulus [15], to others triggered by electrical, ionic and light techniques [16,17].

Among the most successful of these gels, is Polyvinyl Alcohol–Polyacrylic Acid (PVA–PAA), which when suitably treated [12], using water (to produce dilation) and acetone (to produce contraction), replicates on a macroscopic scale the chemical/mechanical energy conversion cycle of organic muscle.

3. Polymer synthesis and response mechanism

Polyvinyl alcohol (PVA) having an 86–89% hydrolysis and an average molecular weight of 100,000 and polyacrylic acid (PAA) with a molecular weight of 500,000–1,000,000 (Fluka AG, Buchs, Switzerland) are separately dissolved in hot water in a ratio of 3:1 by weight, and formed into non-soluble strips (0.1 mm thick, 50 mm wide and 100 mm long) by cross-linking at 150°C for 60 min, following standard procedures [2,12]. During the cross-linking process the polymer

is held under a constant axial load of 5 N. This axial strain serves to align all the long-chain elements during this still mobile stage. Testing of polymers aligned in this way has shown that later dilation is almost exclusively in the axial direction with a resultant reduction in the volume of stimulant absorbed and an increase in the fibre robustness. The reduced stimulant volume serves to reduce chemical wastage and increase efficiency [2]. Polymer strips produced in this fashion formed the standard muscle strip. Any changes to this standard format will be noted in the relevant section of this paper.

At this stage it is important to realise that these polymer gels which form a tangled network immersed in a liquid medium are neither wholly solid nor liquid. The liquid simply prevents the polymer from collapsing into a solid mass, while the network stops the fluid from flowing away. To appreciate the contraction/dilation response it is necessary to understand the forces at work. Three forces have been identified as contributing to the osmotic drive system [18].

1. Rubber elasticity. This arises due to the resistance of the strands to stretching and compression. The rubber elasticity component of the osmotic pressure (the driving force) is [2]:

$$\Pi_r = -(\rho RT\nu_2^{1/3})/M_c \tag{1}$$

where Π_r is the swelling/deswelling force induced by rubber elasticity, ν_2 is the volume fraction (the ratio of the unswollen to the swollen volumes) of the polymer, R is the gas constant, T is the absolute temperature, ρ is the density of the unswollen polymer and M_c is the molecular weight.

2. Hydrogen ion pressure. The hydrogen ion force is associated with the ionisation of the polymer network which releases an abundance of positively charged hydrogen ions into the gel fluid. Although the charge effect is counteracted by negative charges attached to the polymer network, the random motion of the ions causes a pressure in much the same way that air molecules create a pressure in a balloon.

   The osmotic pressure component produced by this effect is:

$$\Pi_e = (\rho RTf/M_c)\nu_2 \tag{2}$$

where f is the number of dissociated hydrogen ions per chain.

3. Polymer–polymer affinity. The third (and in PVA–PAA gels most important) force is polymer–polymer affinity, which arises from interaction between the polymer fibres and the solvent. When the interaction is attractive, as for water, the polymer can reduce its total energy by surrounding itself with solvent molecules, hence water is absorbed. Where the interaction is repulsive, as with acetone, the solvent is excluded. If the water is already locked in the fibre network, the external acetone causes the transfer of water by osmosis through a semi-permeable membrane — the polymer itself.

The polymer–polymer affinity component of the osmotic pressure is given by:

$$\Pi_p = (RT/V)[v^2 + \ln(1 - v_2) + \chi v_2^2], \tag{3}$$

where V is the molar volume of the solvent and χ is the Flory–Huggins parameter. By combining the effects of these three forces the osmotic pressure which holds the gel together may be found. The total osmotic pressure Π_t is given by [19]:

$$\Pi_t = \Pi_r + \Pi_e + \Pi_p \tag{4a}$$

$$\Pi_t = -(\rho RT v_2^{1/3})/M_c + (\rho RTf/M_c)v_2 + (RT/V)[v^2 + \ln(1 - v_2) + \chi v_2^2]. \tag{4b}$$

The thermodynamic relationships which govern these responses have been described elsewhere [2].

4. PVA–PAA performance testing

Although polymeric actuators have a number of attributes that can be said to emulate biological muscle, the key feature is their unique ability to convert chemical energy directly into mechanical motion.

Extensive testing of the polymer and stimulant solvents revealed that a highly desirable response could be achieved by using acetone to cause contraction and 4 molar NaCl solution to produce dilation. This chemical combination has an optimum balance between safety, cost and performance [2].

Since the dynamic rates of contraction/relaxation, and the forces generated during contractile strokes are critical in determining the feasibility of an artificial muscle all properties that might have a bearing on the response must be fully characterised.

A strip of PVA–PAA prepared following the standard format described above was securely anchored at the base of a water tight 'muscle cell'. The free end was connected through a Kevlar tendon to the monitoring sensors which measured the rates of contraction/dilation and the induced forces, Fig. 1.

Water at 21°C was injected into the cell over a period of 0.8 s and the dilation of the muscle was recorded by the position sensor. When fully dilated and in a stable condition the water was removed through a computer controlled exit valve and acetone (17°C) was injected to induce contraction. This alternate stimulation with water and acetone was repeated for several cycles with the results shown in Fig. 2a.

Using the same muscle fibres and with the same basic test configuration the position sensor was replaced by a calibrated loaded cell and the contraction/dilation cycles were repeated. The resultant changes in contractile force during this series of cycles is shown in Fig. 2b.

These initial tests indicated the feasibility of this actuation system in terms of motion and contractile force generation, and revealed that the response was subject to a variety of material factors influencing the dynamic characteristics. The

effects of these features have been characterised in the following sections with the aim of defining the key parameters in the determination of the drive forces and thereby optimising the actuation process.

This initial test system revealed a number of features of the polymer actuator:

1. With a 100 μm muscle, contractile rates of up to 11%/s are possible — well below values for organic muscle. (25–2000%/s is possible but 500%/s is more typical for human skeletal muscle [20].)
2. Using a single fibre with a cross-sectional area of 5 mm^2 a contractile force of 1.45 N could be generated which is equivalent 29 N/cm^2. This is broadly comparable with biological muscle which ranges from 20 to 40 N/cm^2 [20].
3. These results can be repeated over a range of contraction/dilation cycles.

Unfortunately, this performance is not satisfactory for most general actuator applications and overall system performance must be improved. Fortunately during

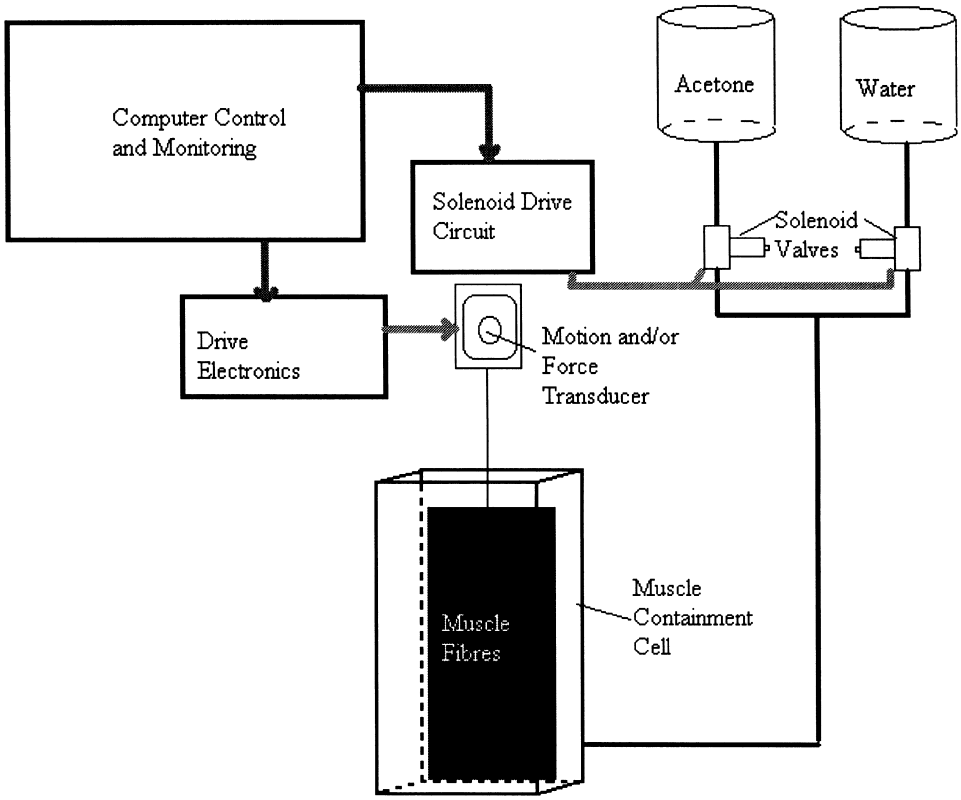

Fig. 1. Schematic of test-cell.

production and testing it was noticed that there are several factors that can influence the response and by manipulating these it was hoped that the necessary improvements could be achieved. These factors are assessed in the following sections.

4.1. Muscle thickness effects

Using the set-up in Fig. 1, testing of contractile rate and force was measured for

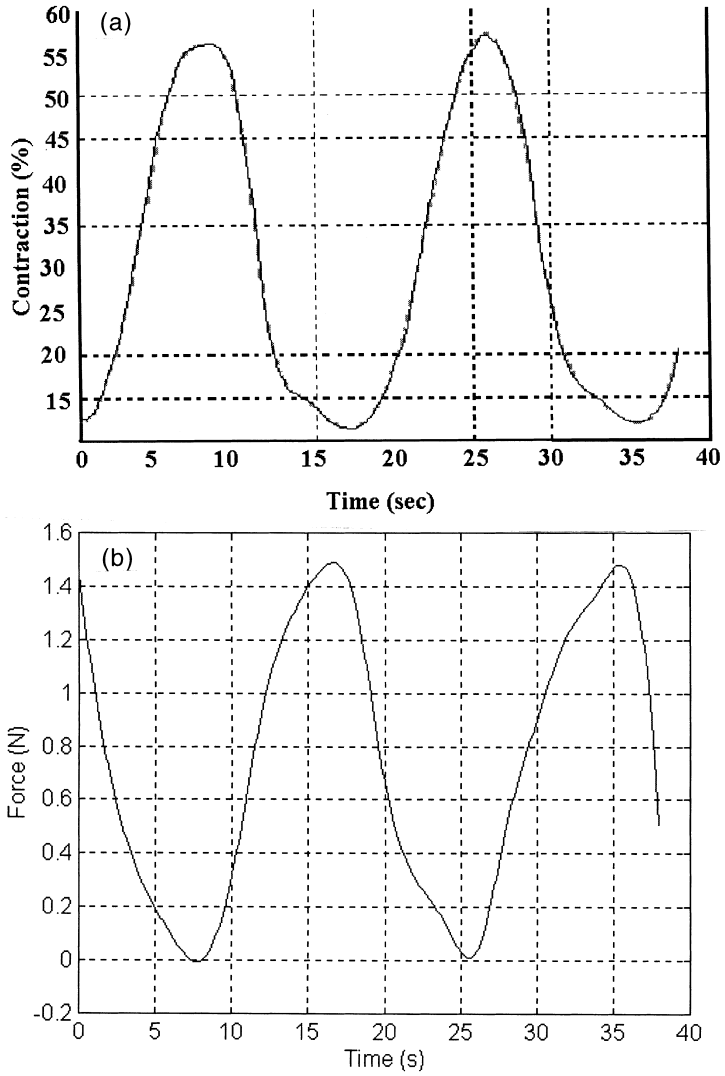

Fig. 2. (a and b) Contractile response for a single strip PVA–PAA fibre.

muscle strips with thicknesses varying from 50 to 500 μm. The recorded responses are shown in Figs. 3a and b.

From these results it can be seen that the fibre thickness does indeed have a strong bearing on both the contractile rate and the force. Indeed, with a 50 μm fibre the peak contractile rate has now risen to 43%/s, which is now becoming comparable with some slow acting biological muscle. The relationship between the film thickness and the response rate is given by:

$$\phi = K_d/\tau^2 + C_d \tag{5}$$

where ϕ is the contractile rate, τ is the fibre thickness and K_d and C_d are constants set during the production of the polymer and determined by the ratio of PVA to PAA and the crosslinking period and temperature [2].

Unfortunately and not unexpectedly, there is also a reduction in the contractile force as the thickness is reduced, with the force on a 50 μm fibre now only 0.75 N. The positive feature of this data however, is that despite the overall reduction in the measured force, the force/cm^2 remains constant at 30 N/cm^2.

As a compromise between the need for rapid response and contractile force, a new muscle bundle was constructed from ten 'standard' but 50 μm thick fibres, connected in parallel. The results for these ten fibres are also recorded in Figs. 3a and b, from which it is clear that there are no significant effects on the contractile rate but now the contractile force has been increased by a factor of 9.7 (thereby maintaining the contractile force/cm^2). This is a response typical of biological muscle, where increased muscle bulk (more fibres) gives a proportionately increased force.

It should also be noted that the nature of the fibre (100 mm long by 50 mm wide) means that diffusion of the stimulant into the fibre is almost exclusively one dimensional. In muscle fibres which are fundamentally cylindrical, chemical diffusion is two-dimensional with a resultant improvement in performance [2,21]. Production of multi-stranded hair-like PVA–PAA fibres is currently not a viable alternative, but should provide some further improvement in the contractile response at the cost of a much increased number of hair-like fibres in an actuator bundle.

4.2. Thermal effects

The temperature of the system was also believed to have a fundamental effect on the performance. This was tested by varying the temperature of the input solvents from 5 to 45°C. The resultant changes in the contractile rate and the force are shown in Figs. 4a and b.

From these results it can be seen that increasing the thermal energy increases activation activity. This is comparable on a gross scale with increased biological muscle activity with increased temperature, although the synthetic muscle clearly has a much greater thermal operating range. The changes in contractile response with temperature are governed by:

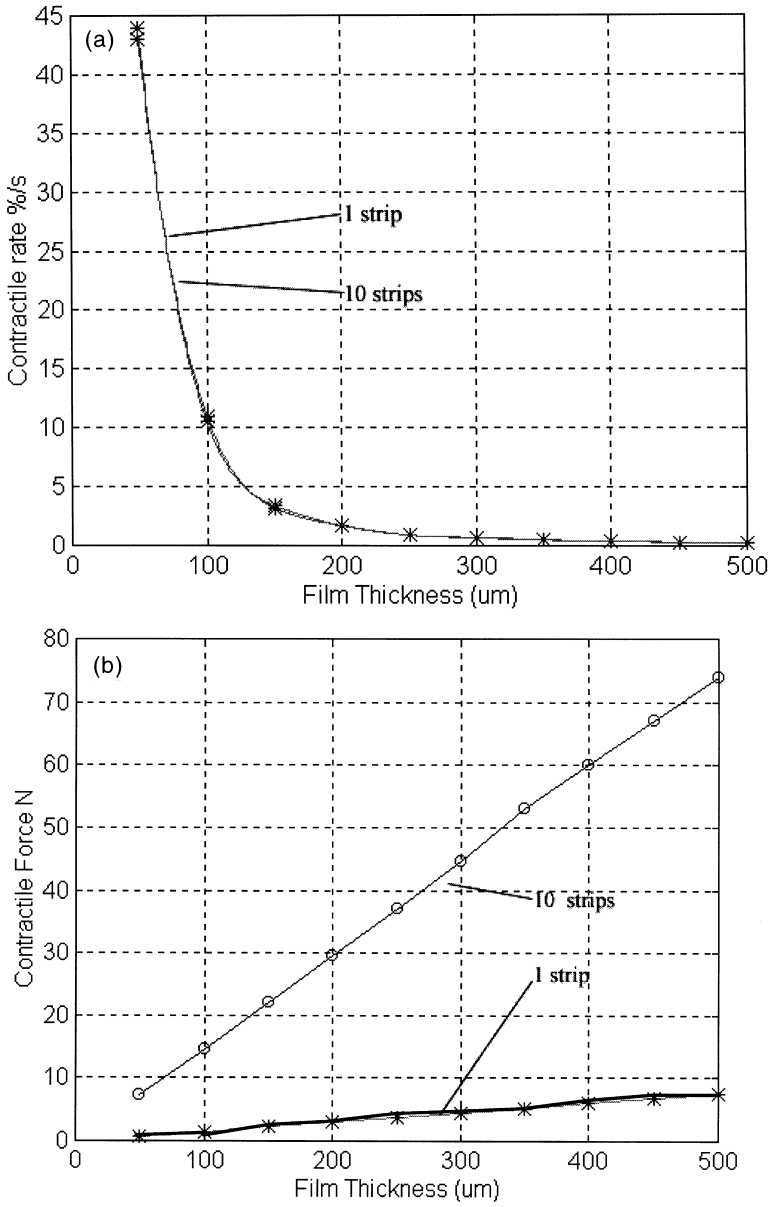

Fig. 3. (a and b) Effects of fibre thickness on contractile rate and force.

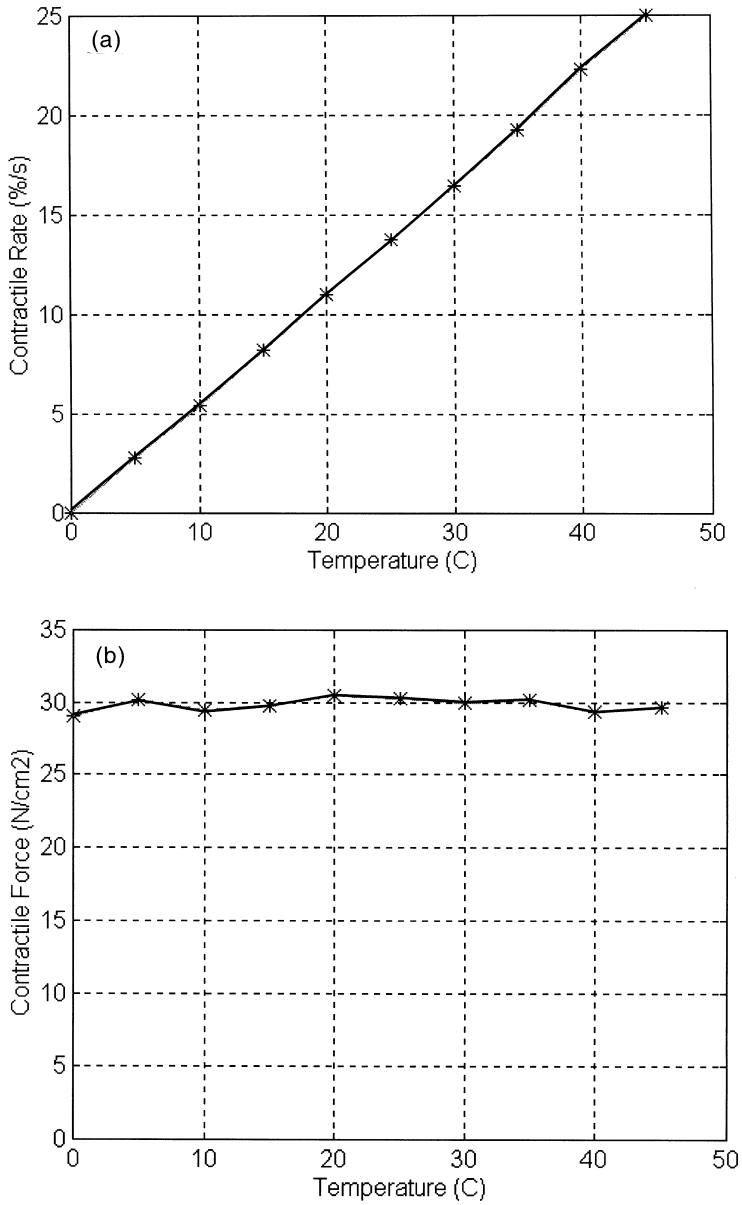

Fig. 4. (a and b)Effects of solvent temperature on contractile rate and force.

$$\phi = \phi_{20} + K_t T_\rho \tag{6}$$

Where ϕ_{20} is the contraction (or swelling) rate at 20°C, K_t is the contractile coefficient and T_ρ is the temperature above 20°C.

From these results it can be seen that temperature has a very significant effect on the response with a doubling of the contract rate for a 40°C rise in temperature. This gives a new maximum contractile rate for a 50 μm strip with the solvents at 45°C, of almost 75%/s, again a very significant and important increase. Unfortunately due to three factors much lower temperatures had to be used:

1. Above 40°C the fibre structure starts to deform plastically.
2. The raised temperature creates a large increase in acetone fumes with the associated dangers.
3. Heating the solvent requires care and considerable energy input.

Having shown that elevated temperature could be used for improved performance all future tests were conducted at room temperature (21°C).

The contractile force remains unchanged across the 5–45°C range although of course the time to reach the maximum contractile force varies. Above 45°C where plasticising of the polymer occurs there will possibly be contractile force changes but this was not tested due to safety concerns.

4.3. Solvent concentration effects

Polymers prepared as described previously were allowed to fully dilate in a 4 M NaCl solution until a stable condition was attained. The water solution was drained and acetone solutions with concentrations from 100 to 0% were injected into the cell. The resultant peak contractile rates and contractile forces were recorded in Figs. 5a and b.

From the results it is clear that any contamination of the chemical stimulant significantly effects the performance. At the same instance knowledge of this contamination factor can be used to control the contractile velocity in addition to the previously controlled contractile (position) limits.

The change in the contractile rate due to contamination is given by

$$\phi = e^{(-23.5x^2)} \tag{7}$$

where x is the contaminant fraction in the solution.

4.4. Force/velocity profile

Since a polymeric muscle is designed to emulate the behaviour of organic muscle it is reasonable to attempt some comparison of their behaviours. In terms of biological muscle, characteristic behaviour is often summarised in the classic force–velocity curve which shows the intrinsic relationship between the muscle contractile force and the velocity of contraction, measured through a series of isometric and isotonic tests [3].

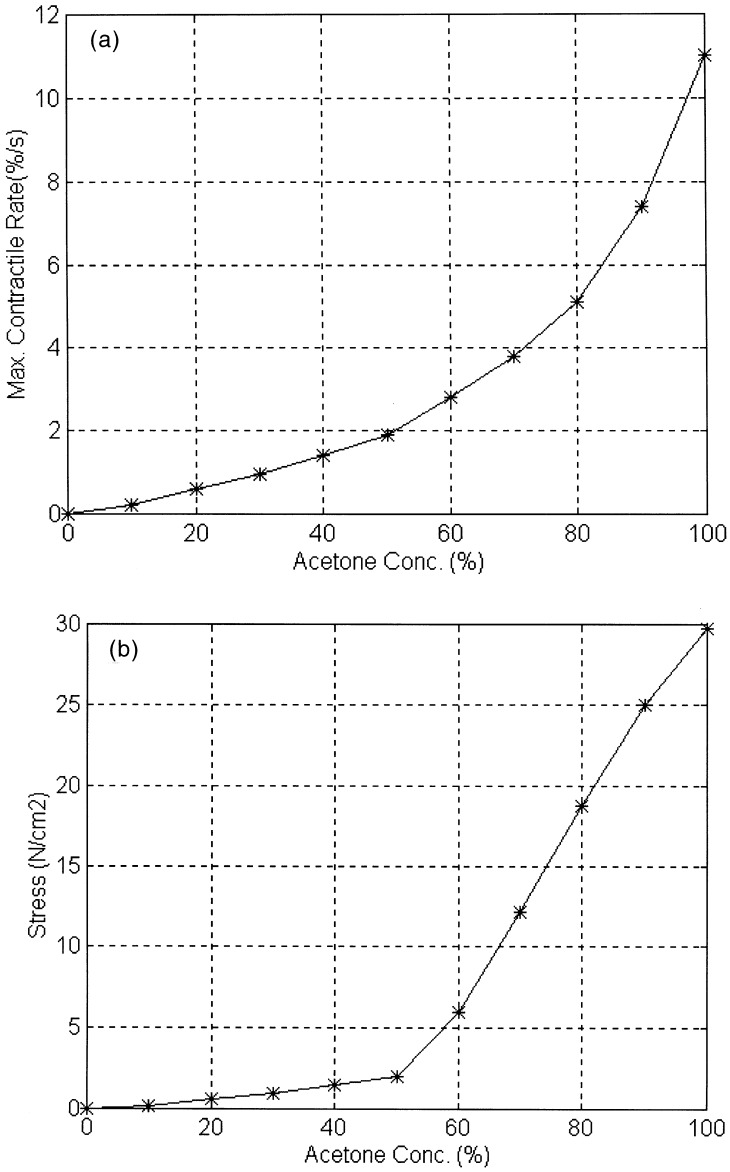

Fig. 5. (a and b) Effects of solvent concentration on contractile rate and force.

4.5. Isotonic tests

The following profiles have been prepared for a bundle of 10, 50 μm fibres operating at 21°C. As the muscle fibres are still relatively small only light loading was imposed on the system. The loading on the muscle was varied from 0 to 6 N and the resultant peak contractile rate was measured for each muscle fibre bundle. During these tests the effects of over-loading were also investigated.

4.6. Isometric tests

Using the standard muscle fibre in 10 strips as defined previously. The muscle cell was attached to the load cell, which had been off-set to record zero with the muscle in the fully dilated condition. From this fully dilated condition contraction was induced by the introduction of acetone and the resultant force profile during the contraction–dilation cycles was recorded. From these results a maximum force of 15.5 N was recorded which gives a contractile force of 31 N/cm^2. Repeated test on the contractile force showed that the forces after 30 cycles were 15.5 ± 0.5 N (31 ± 1 N/cm^2). This was repeated at different muscle pre-tension lengths.

Using the isometric and isotonic data obtained above a force/velocity profile can be generated and compared with natural muscle, Fig. 6. The results have been normalised to maximum force and contractile rate values so that a comparison can be made of the profile forms, without comparison of the physical rates which are still widely separated. From these profiles there are clearly distinct similarities in the response format and therefore in the actuator functionality.

4.7. Power output

In all actuators a further important measure of the performance is the power profile. When measurements of the mechanical performance of muscles are compared it is often desirable to eliminate variations due to size, shape, and the contractile components. Although many such arrangement are possible, this work has concentrated on fibres arranged as parallel strips connected at common binding points. This is a model readily applicable to some forms of natural muscle.

Since the shortening velocity adds up along the fibre, it is proportional to the muscle length and the normalised contractile velocity can be given by

$$V_{\text{norm}} = V/l_{\text{f}} \tag{8}$$

where l_{f} is the muscle fibre length, V is the velocity of shortening (contractile rate) and V_{norm} is the normalised velocity of shortening per unit length. With the fibres in parallel, the force generated is proportional to the cross-sectional area of the fibre, and the normalised force is;

$$F_{\text{norm}} = F/A \approx Fl_{\text{f}}/vol \tag{9}$$

where vol is the volume of the dry muscle fibre, F is the force generated, A is the

cross-sectional area, and F_{norm} is the normalised force per unit volume. The power of this actuator can be obtained from the velocity and force values. The normalised power output P_{norm} is

$$P_{norm} = F_{norm} V_{norm} = FV/vol. \tag{10}$$

This power output equation is valid for all other possible arrangements of the fibres, although the velocity and force measurements may vary considerably. The power produced by any muscle either natural or artificial can therefore be derived from the information in the force/velocity profile and maximum power is found to be achieved when $P_{norm} = F_{norm}$.

For the PVA–PAA muscles tested here, the maximum power was found to be 21 mW/g (21 W/kg) which is much less than for biological muscle (40–250 W/kg). Fortunately this is not too dismaying as the power is the product of the force (which is constant for a constant cross-sectional area) and the contractile velocity which increases as thickness decreases. Hence, theory predicts that thinner hair-like strands could achieve an acceptable power output.

4.8. Muscle elasticity limits

In the fully dilated state the muscle loading was increased from 0 to 70 N/cm^2 and the resultant stress recorded, Fig. 7. It was noted that for stress of less than

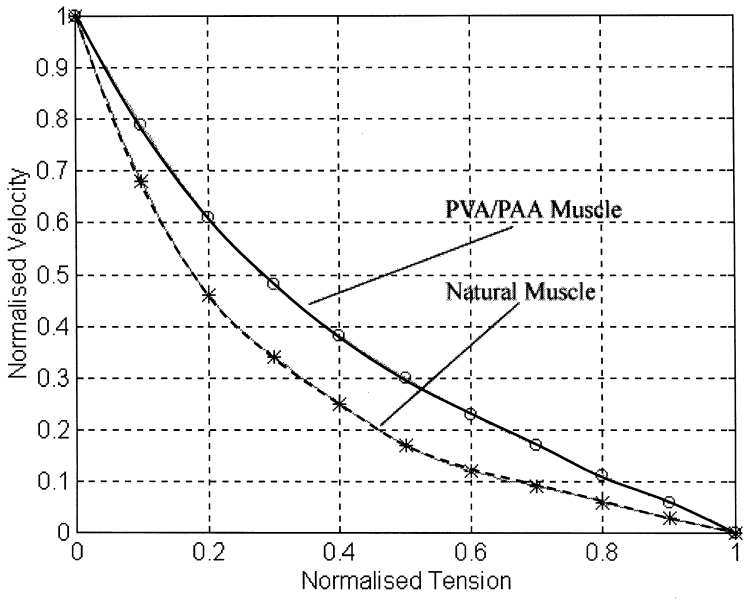

Fig. 6. Force/velocity profiles.

39.5 N/cm^2 the fibres returned to their original condition with no detriment to the performance. With loading from 42 to 60 N/cm^2, relaxation of the loading showed plastic deformation had occurred, but the muscle performed as previously determined with a new baseline zero contraction point, i.e. the muscle was longer at zero than previously recorded. With a loading above 60 N/cm^2 the muscle strips were destroyed.

4.9. Carnot cycle

As a final comment on the performance of polymer muscles as an actuator, it is useful to consider the work cycle that is involved. This is based on the Carnot cycle for ideal cases.

For a mechanochemical cycle the driving force is the chemical potential of the stimulant solvents, with variations being plotted as changes in polymer length and force. This requires a four-stroke operation.

Starting at {1}, water/NaCl is added to the system causing expansion against no external forces {1}–{2}. At {2}, the NaCl solution is removed and an external force is applied causing an increase in force and extension {2}–{3}. The force is kept constant at {3}–{4}, but the chemical potential is changed by the addition of acetone. Here contraction occurs against a constant load. Finally the external force is reduced to zero and the force/extension relationship returns to its original position by {4}–{1}. The energy changes for each step can be given as:

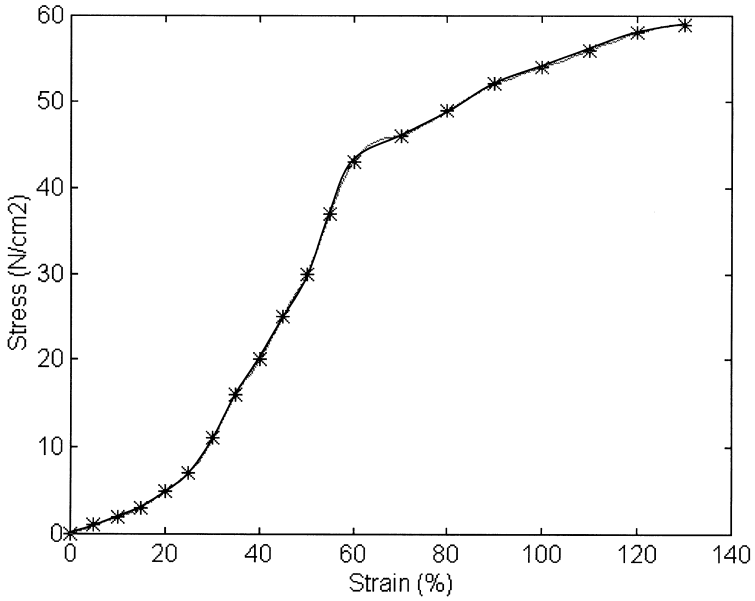

Fig. 7. Stress/strain curves.

$$[\mathrm{d}H]_{\{1\}-\{2\}} = [\mu_{\mathrm{H20}}]_{\{1\}-\{2\}}$$

$$[\mathrm{d}H]_{\{2\}-\{3\}} = [F\,\mathrm{d}l]_{\{2\}-\{3\}} + [\mu_{\mathrm{H20}}]_{\{2\}-\{3\}}$$

$$[\mathrm{d}H]_{\{3\}-\{4\}} = [F\,\mathrm{d}l]_{\{3\}-\{4\}} + [\mu_{\mathrm{ACE}}\mathrm{d}n_{\mathrm{ACE}}]_{\{3\}-\{4\}}$$

$$[\mathrm{d}H]_{\{4\}-\{1\}} = [F\,\mathrm{d}l]_{\{4\}-\{1\}} + [\mu_{\mathrm{ACE}}\mathrm{d}n_{\mathrm{ACE}}]_{\{4\}-\{1\}}$$

where μ is the chemical potential, dn is the number of ionic groupings in the solvents, H is the Helmholtz energy and dl is the displacement change in the material under an external force F.

From these results it is seen that steps {1}–{2}–{3} represent the work done on the fibre to cause dilation, while {3}–{4}–{1} is the contractile work that the system performs.

Clearly the polymer pseudo muscular actuator is capable of replicating many aspects of organic muscle function, and at the same instance has valuable mechanical actuator benefits. These attributes will be compared and assessed in a later section.

5. Pneumatic muscle actuators

5.1. Construction

Pneumatic Muscle Actuators (pMA) derivatives of the McKibben muscles developed in the 1950s and 60 s, [5], are constructed as a two-layered cylinder, Fig. 8. The inner layer is made from butyl rubber tubing, with two end-caps forming the termination connectors to seal the muscle cylinder. These end-caps can be made of nylon, aluminium, brass, steel or indeed any material depending on the specific operational requirements. As the majority of the mass of the actuator is in the end-cap, savings in this area have a very significant effect on the measured power and force to weight ratio. One of the end-caps is sealed, closing the muscle cylinder, while the other acts as the air input conduit. Around the rubber tubing there is a flexible outer sheathing formed from high strength interwoven (but not bonded) nylon fibres. The sealed rubber/nylon cylinder acts as a pressurised containment unit. The flexibility of this structure means that it can be stretched or compressed without damage, but at the same time this shell prevents the delicate rubber liner from over-inflating and rupturing. To prevent energy losses due to the initial expansion of the rubber liner, the rubber layer has a diameter comparable with the rest diameter of the flexible wall. The muscles are available in a number of sizes providing variable force potential and actuator displacement ranges.

This combined rubber–braided nylon forms a transmission path to convert the radial expansive forces into axial contractile forces.

It is important to note that although the input of air to the muscle chamber increases the volume of the muscle cell this actually induces a contractile force which is the main drive of these actuators.

pMAs can be constructed in a range of lengths and diameters with increases in sizes producing increased contractile force and/or displacement. Muscles lengths can range from under 10 to 400 cm and diameters range from 10 to 70 mm.

5.2. System model

The factors critical in the determination of the driving force in any pneumatic system are the pressure difference and the area over which a distortion pressure is applied. With conventional cylinders only the piston face plate is free to move and only this area is critical. In the braided muscle the flexibility of the structure means the whole shell/liner interface forms the transfer medium for the actuation force. The braided structure of the external nylon shell means that the muscle may be considered as a series of two-dimensional trapezoids. In this design, as the actuator stretches or compresses the interweave angle will change and the whole surface area of the muscle varies. To determine the driving force it is therefore essential that the surface area at any interweave angle or length be known [22,23].

To calculate the contraction force, the following transition from state 1 (P, V) to state 2 (P, $V + \mathrm{d}V$) is considered. The pressure inside the pMA is considered to remain constant during the transition. The pneumatic energy stored during the transition can be obtained from the surface below the transition curve shown in the (P, V) diagram (Fig. 10).

This input pneumatic energy induces two force components. The contractile force component F_{cont} and the expansion force component F_{exp}. The contraction force is produced by the pressure on the side surface of the pMA while the expansion force is created due to the pressure on the end cap surface.

$$F_{\mathrm{mus}} = PS_{\mathrm{mus}} \tag{11}$$

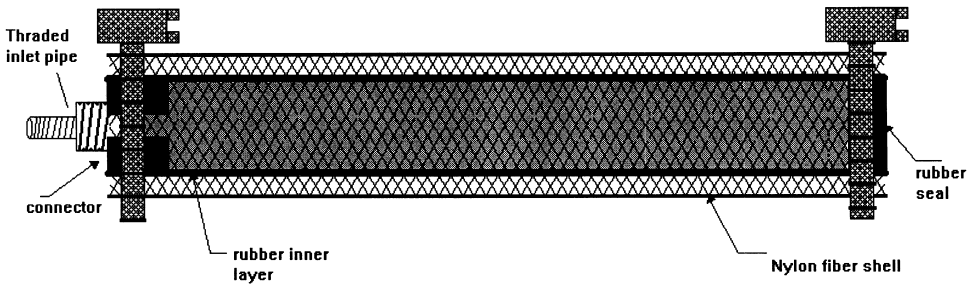

Fig. 8. Basic pneumatic Muscle Actuator design.

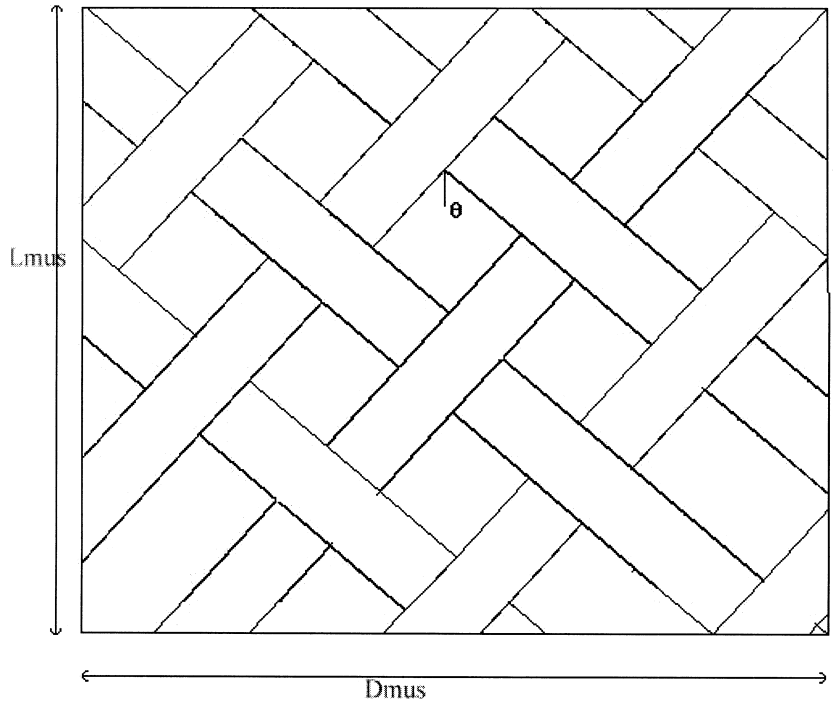

Fig. 9. Trapezoidal nature of the muscle braid.

$$F_{\text{cont}} = aF_{\text{mus}} \tag{12}$$

$$F_{\text{exp}} = PS_{\text{cap}} \tag{13}$$

Where S_{mus} is the muscle body surface area, S_{cap} is the end cap surface area and α is a conversion factor between the radial force induced by the pressure on the muscle body surface and the resultant contractile force. This is determined later in this section. Therefore, the actual driving force will be given by

$$F = F_{\text{cont}} - F_{\text{exp}} . \tag{14}$$

Considering an ideal cylinder the muscle side surface area and the cap surface area are

$$S_{\text{mus}} = \pi D_{\text{mus}} L_{\text{mus}} = \frac{h^2 \ \sin(\vartheta)\cos(\vartheta)}{B} \tag{15}$$

where $L_{\text{mus}} = h\cos(\vartheta)$ and $D_{\text{mus}} = (h\sin(\vartheta)/B\pi)$ are the length and the diameter of the muscle as a function of the helical fibre length h and the number of trapezoids B, Fig. 9.

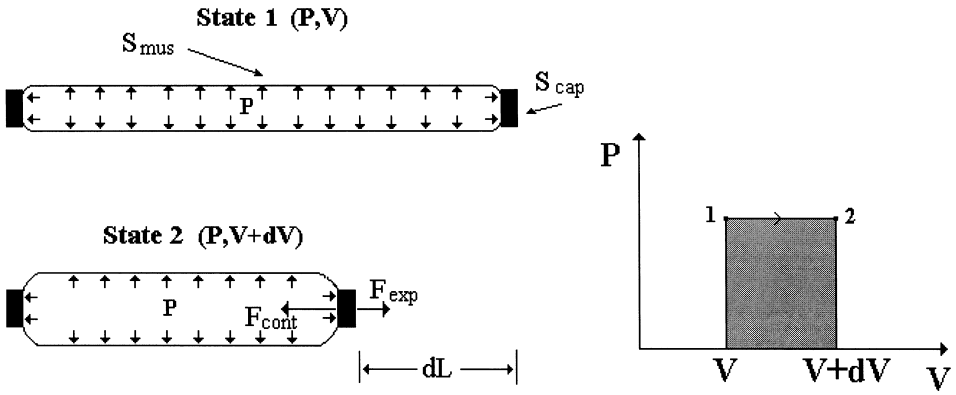

Fig. 10. Actuator transition states.

$$S_{\text{cap}} = \frac{\pi D^2}{4} = \frac{h^2 \sin^2(\vartheta)}{4B^2\pi} \quad \text{if } D_0 \sin \vartheta > D_{\text{cap}} \quad \text{or } \vartheta < \sin^{-1}\frac{D_{\text{cap}}}{D_0} \tag{16}$$

where D_0 is the theoretical maximum muscle diameter for braided angle $\vartheta = 90^\circ$. In this case the muscle diameter D is bigger than the cap diameter D_{cap}. In case that a large cap is used then for braided angle $\vartheta < \sin^{-1}(D_{\text{cap}}/D_0)$ the muscle diameter D becomes smaller than the D_{cap}. In such a case the S_{cap} surface of cap disk and will be given by

$$S_{\text{cap}} = \frac{\pi D_{\text{cap}}^2}{4} \quad \text{if } \vartheta < \sin^{-1}\frac{D_{\text{cap}}}{D_0}. \tag{17}$$

To calculate the actual contraction the conversion factor α must be computed. The conversion factor α is calculated using the conservation principle between the work done by the radial force and the work done by the contractile force, Fig. 11. The work produced by the radial force $\mathrm{d}F_{\text{mus}}$ is given by

$$\mathrm{d}W_{\text{mus}} = F_{\text{mus}}\, \mathrm{d}D \tag{18}$$

where $\mathrm{d}D$ is the body surface displacement.

The work produced by the contractile force will be given by

$$\mathrm{d}W_{\text{cont}} = F_{\text{cont}}(-2\, \mathrm{d}L). \tag{19}$$

Assuming the energy conservation principle we can write that

$$\mathrm{d}F_{\text{cont}} = \frac{\mathrm{d}D}{2\, \mathrm{d}L}\, \mathrm{d}F_{\text{mus}} = \alpha\, \mathrm{d}F_{\text{mus}} \tag{20}$$

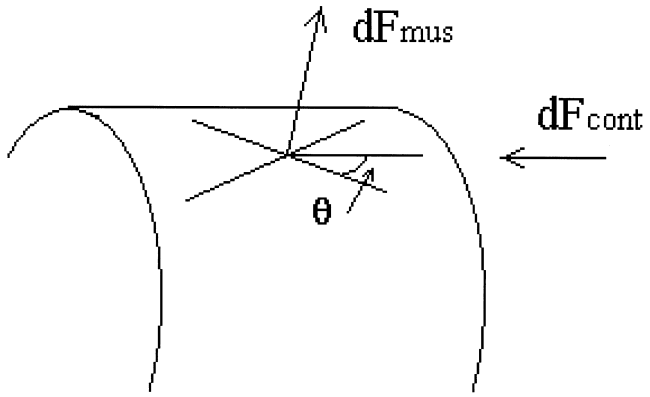

Fig. 11. Radial/contractile force relation.

$$\alpha = \frac{\mathrm{d}D}{-2\ \mathrm{d}L} = \frac{1}{2B\pi\ \tan(\vartheta)}. \tag{21}$$

Substituting into Eq. (14) the formula of the actual driving force of the actuator is obtained

$$F = \frac{Ph^2 \cos^2(\vartheta)}{2B^2\pi} - \frac{Ph^2\ \sin^2(\vartheta)}{4B^2\pi} \tag{22}$$

$$F = \frac{\pi D_0^2 P}{4}(3\ \cos^2\theta - 1) \quad \text{if } \vartheta > \sin^{-1}\frac{D_{\mathrm{cap}}}{D_0} \tag{23}$$

$$F = \frac{\pi P}{4}(2D_0^2\ \cos^2\theta - D_{\mathrm{cap}}^2) \quad \text{if } \vartheta < \sin^{-1}\frac{D_{\mathrm{cap}}}{D_0}. \tag{24}$$

The above equation for $\vartheta > \sin^{-1}(D_{\mathrm{cap}}/D_0)$ is identical with the one obtained by Chou et al [23]. However (23) does not consider the surface area of the end-cap which can result in a reduction of the driving force when the actuator approaches its maximum length. This effect is clearly illustrated in the simulation results for a muscle with $D_0 = 0.07$ m, $D_{\mathrm{cap}} = 0.032$ m Fig. 12.

6. Actuator performance assessment

The basic test system used for the assessment of the muscle parameters is shown in Fig. 13. The rig consists of a mechanical support to which muscles can be mounted and easily adjusted for length and tension, a strain based sensor to detect the strain in the muscle during loading, a position sensor to monitor the length of the muscles, a servo input valve with external closed loop pressure

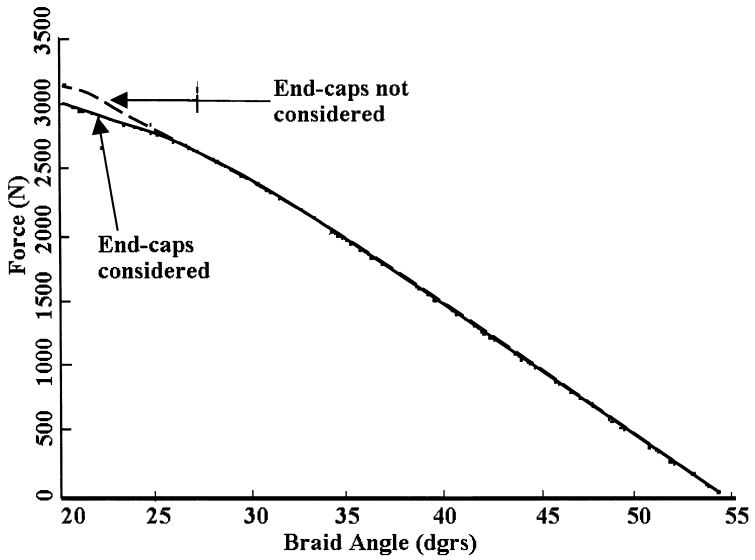

Fig. 12. Theoretical effect of D_{cap} on the maximum Actuator force.

control and a PC with data acquisition hardware. As with the polymeric actuator a series of isotonic and isometric tests were conducted for comparison with the force theory above.

Tests were conducted on a fairly large muscle which having large forces and dimensional changes helped to reduce the potential error sources. The muscle tested has a fully extended length of 1.77 m and a fully contracted value of 1.18 m. This gives a dimension change of 33% which is typical of this type of actuator. This muscle has aluminium end-caps, an overall mass of 530 g and a diameter of 25 mm. The fully contracted muscle diameter is 55 mm while the measured value for h is 72 mm. During testing the pressure was varied from 0 to 500 kPa. The air flow rate is up to 4 l/s. The muscle has been pressure tested to 800 kPa but the input pressure was limited due to concerns for the structural integrity of the test rig. The maximum measured force at an operating pressure of 500 kPa was 2490 N.

The results of the force and displacement profiles with pressure are shown in Fig. 14(a) and (b). An interesting and surprising observation was the almost total lack of hysteresis. During initial testing hysteresis was indeed observed as noted by other researchers [23], however, adjustment to the location of the sensor recording the in-muscle pressure revealed that these initial readings were more indicative of the pipe and valve pressure than the true pressure in the muscle. These performance tests were undertaken for calibration of the actuators prior to installation in a prototype rig for a nuclear retrieval and clean-up application [24].

This procedure involved automation of the control and actuation of a 50 kg

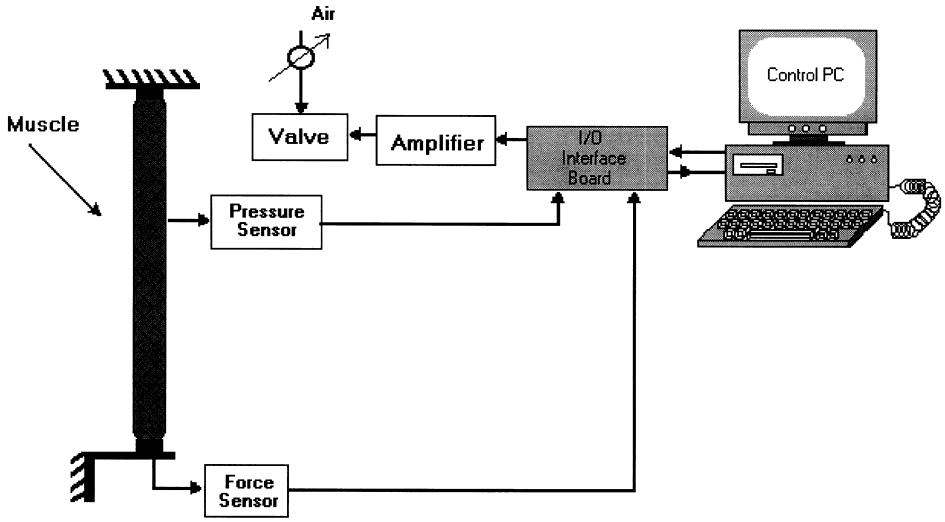

Fig. 13. pMA test system.

manipulation pole used for grappling applications for nuclear waste retrieval from storage pods, Figs. 15a and b.

The mechanical superstructure for this project consisted of basically pyramidal support frame mounted over the storage pond with a 7.5 m long 50 kg grappling pole freely supported at the peak of the pyramid by a spherical joint, Fig. 15a. Four actuators as specified in the above test are used in this application and are mounted between the superstructure and the manipulation pole. Figure 15b shows one of the two axes of this arrangement.

7. System testing and results

To test the effectiveness of these actuators in a practical application a number of performance assessments were undertaken [24].

1. Basic Actuator Performance testing (Work Volume and Loading): This simple test was required to verify that the designed pMA system could move the pole and a load (combined mass 50 kg) through a work volume measuring 3×3 m at the pole tip. Direct measurement of the motion revealed that this could easily be achieved satisfying the power and motion range requirements.
2. Fine Motion testing: The initial design specification required a pole tip resolution and fine motion control of 3 mm. A series of fine step motions (3 mm) were introduced to test the ability of the system to respond to small motions and also to locate the pole tip at 3 mm steps. The test results are illustrated in Fig. 16 and show that the controller could successfully move the

tip of the 7.5 m pole in 3 mm steps according to the initial design specifications of the system. A small delay was noticed when the system motion was reversed. This step delay on reversing the direction of motion is caused by some wind-up in the controller.

3. Stability/Performance testing: An important specification of the system was for stability across the operational environment to both large and small motion inputs. To test the stability and the quality of the system response a series of step inputs were introduced. Motions for a small 3 mm step have already been

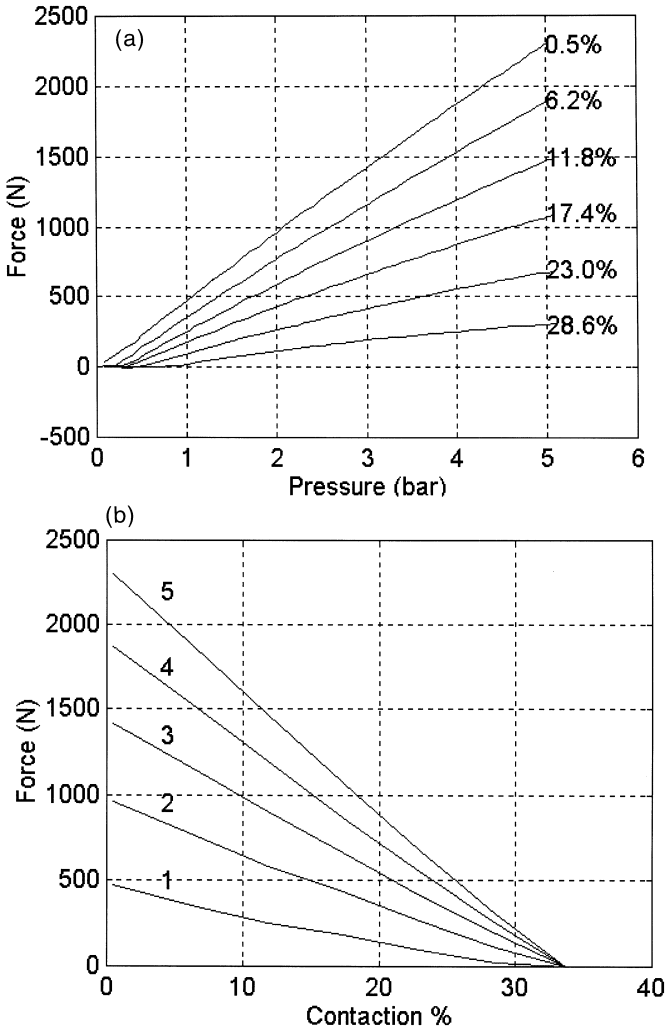

Fig. 14. (a) Force/pressure profiles. (b) Force/displacement profile.

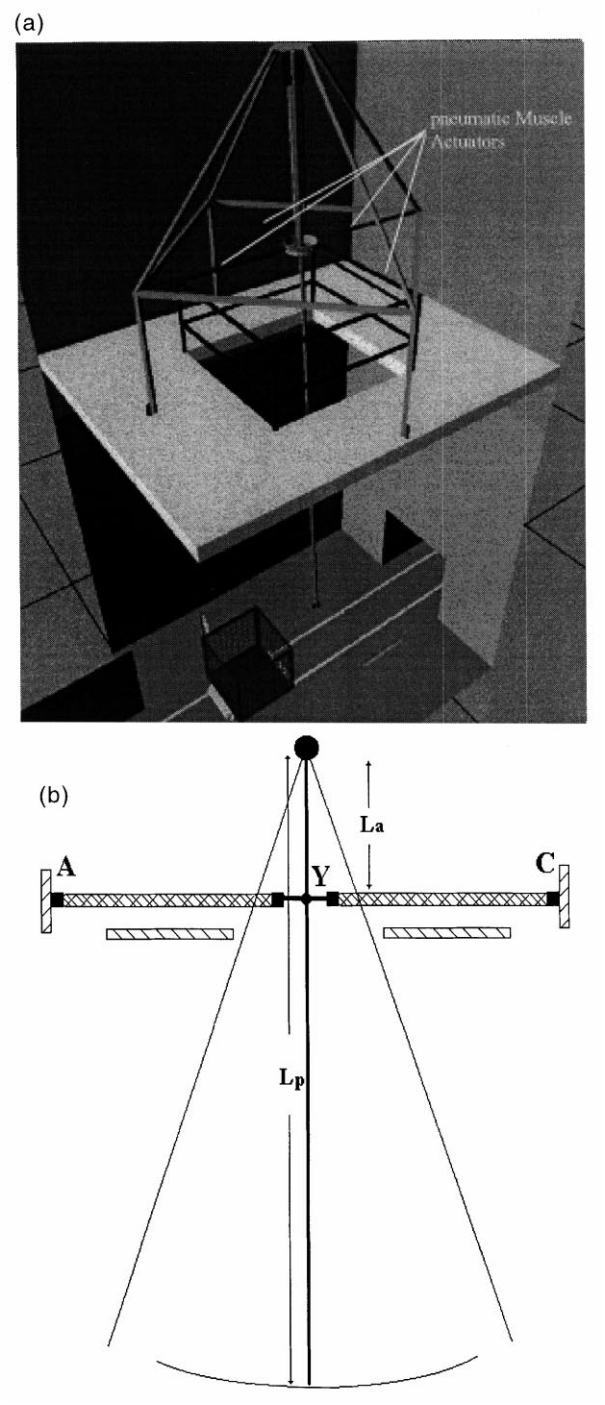

Fig. 15. (a and b) Actuation system schematics.

shown, while typical results for a 1 m step are shown in Fig. 17. Analysis of these results permitted tuning of the system's PID controllers. The final system controller values were set from these results based on a MATLAB developed control scheme.

4. Bandwidth testing: To test the bandwidth of the system a series of sinewave inputs of varying frequency were introduced from the control computer. For the specified work volume (3 × 3 m) the bandwidth was found to be approximately 0.05 Hz as shown in Fig. 18. Although this appears low, this is

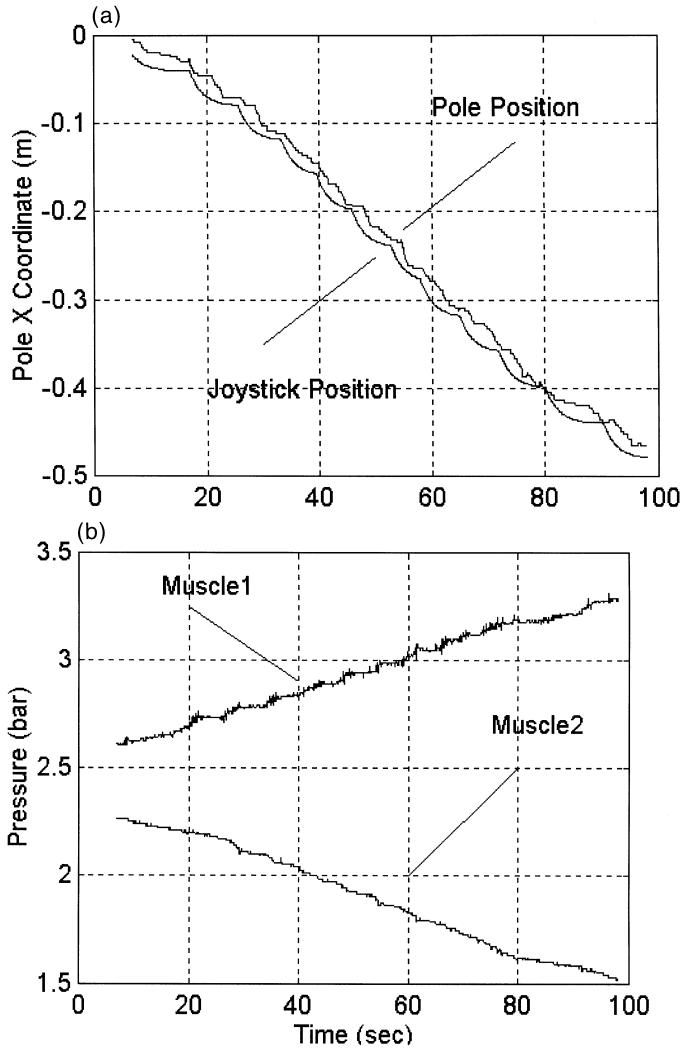

Fig. 16. (a) System response to fine motions (motion step = 3 mm), (b) antagonistic muscle pressures.

better than the initial specification parameters based on human operator work cycles.

Using the data from the above tests, practical implementation and previous laboratory tests on smaller actuators [25], it is possible to present details of the performance specifications of these actuators.

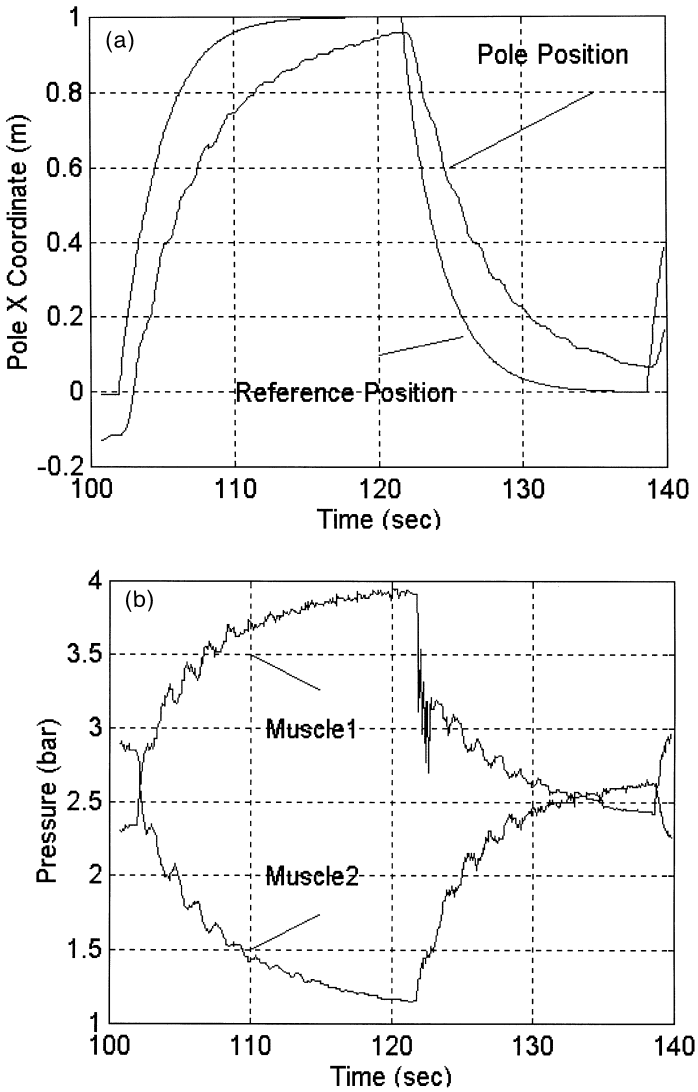

Fig. 17. (a) System 1 m step response — filtered, (b) antagonistic muscle pressures during the system response.

7.1. Force and power/weight

For pMAs the actual force/weight and power/weight ratio is highly muscle dependent. Factors of influence are the weight of the end-caps, the weight of the rubber/nylon braid (which is usually negligible), the operating pressure (in most tests this is limited to 5 bar but much higher pressures are possible with a linear

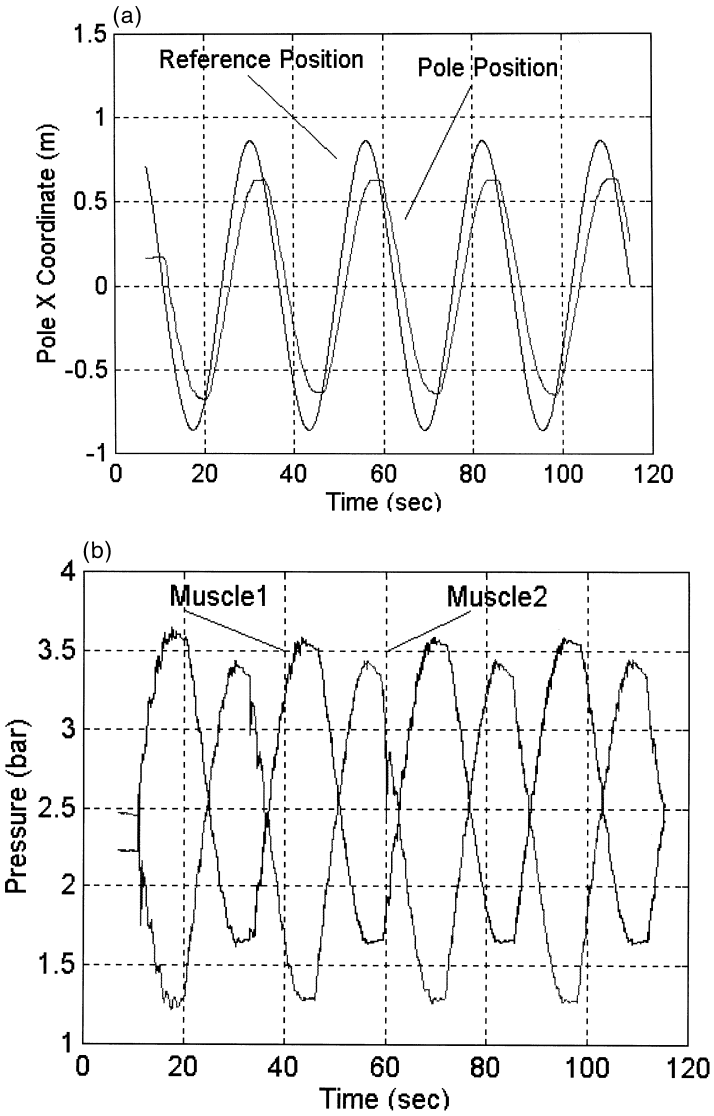

Fig. 18. (a) Response to a sinusodial input (frequency ~ 0.05 Hz), (b) antagonist muscle pressures for a sinusoidal input.

increase in force) and the dimensions of the muscle. The most important factor in the power/weight performance is in fact the air flow rate which acts as a limit on the rate at which pneumatic power can be delivered. It is therefore vital when quoting the power/weight that flow rate also be stated. Based on the air supply of the device studied above a power weight ratio of 800 W/kg was achieved at an air flow rate of 3 l/s. For smaller devices with nylon end-caps power/weight values of 1–2 kW/kg have been recorded.

The force/cm^2 of cross-sectional area is over 100 N/cm^2 at full contraction (the worst case) while in the best case (fully dilated) it is over 500 N/cm^2.

7.2. Displacement

The actual achievable displacement (contraction) is dependent on the construction and loading but is typically 35% of the dilated length or over 50% of the contracted length.

7.3. Systems control

Development of adaptive controllers for these air control systems have shown that muscles can be controllable to an accuracy of better than 1% of displacement. Bandwidths for antagonistic pairs of muscles of up to 5 Hz can be achieved (10 Hz for a single muscle). Where very large muscles and loadings are present much lower bandwidths are obtained limited primarily by the air flow rate. Force control using antagonistic pairs of muscle has also been demonstrated with control to 1% of full scale over a range from 10 to 4000 N. As the size of the muscle is increased and the flow rate limits become more apparent the bandwidth of the device reduces.

When operated with these adaptive controllers it has been demonstrated that the muscles can rapidly adapt to structural changes and pressure losses caused by damage to the system.

7.4. Efficiency

The efficiency of conversion of pneumatic energy to mechanical motion as with most apsects of the operation is dependent on the exact muscle construction but typical conversion values are from 30 to 50% efficient.

8. Conclusions

In this paper a study has been undertaken of two novel forms of actuators which have characteristics that can be broadly classified as giving them a range of bio-mimetic functions. At the same instance for the pneumatic Muscle Actuator a practical engineering scenario has been described. Through this it is hoped that the beneficial features of biological muscle and mechanical actuators can be

combined and compared. In concluding this study a comparison of the relative performance characteristics of organic muscle, pseudo muscular actuators and pneumatic Muscle Actuators has been made, Table 1, permitting some analysis of the needs for muscle-like systems, their benefits and their limitations.

From this data it can be seen that in many respects polymeric muscles can be competitive with the biological muscle. The major limits on this technology, however, relate to the feasibility of long term large scale use. Polymeric muscles have only been produced in small quantities and as the number of fibres increase there may be difficulties with the stimulant delivery. In addition these muscles have not been tested for extended periods and at present long term cycling is difficult due to the cost of the stimulant (acetone), disposal of the waste, and general robustness of the fibres.

pMAs when compared with biological muscle appear to be even more appealing. In terms of most mechanical performance measures they are comparable, superior and in some instances vastly superior to the natural muscle. They can be accurately controlled, operate over a fairly high temperature band and have inherent properties of compliance/impedance control. In addition, industrial testing is starting to reveal the robustness characteristics which are good, although not impressive when compared with the regenerative behaviour of natural muscle. In addition, pMAs have even demonstrated a good level of scalability. From this analysis it is clear that pMAs have many attributes needed in biological muscle and could indeed be viable bio-mimetic systems. The only significant variant feature is the use of pneumatic as opposed to chemical energy

Table 1
Comparison of organic and artificial muscles

Parameter	Biological muscle	Polymeric muscle	pMA muscle
Displacement	35%	45%	35%
Force/cm^2	20–40 N	30 N	100–500 N
Power/weight	40–250 W/kg	21 W/kg	500–2 kW/kg
Efficiency	45–70%	30–40%	32–50%
Rate of contraction	25–2000%/s	75%/s	35–700%/s
Control	Good	Low–fair	Fair–good
Operation in water	Yes	Partially	Yes
Temperature range	0–40°C (unclothed)	0–40°C	−30 to +80°C
Robustness	Excellent	Poor	Fair–good
Self repair–regeneration	Yes	No	No
Antagonistic operation	Yes	Yes	Yes
Compliance/impedance control			
Energy source	Chemical	Chemical	Pneumatic
Environmental safe	Produces CO_2	Uses acetone	Yes
Scalable	μm–m	–	cm–m
Linear operation	Yes	Yes	Yes

and the resultant problems of effective energy storage. This is clearly an area that needs to be addressed for the future.

References

[1] Inoue H. Whither robotics: key issues, approaches and applications. In: IROS '96, Osaka, Japan, 1996. p. 9–14.
[2] Caldwell DG, Taylor PM. Chemically stimulated pseudo-muscular actuation. Int J Eng Sci 1990;28:797–808.
[3] Hollerbach JM, Hunter IW, Ballentyne J. A comparative analysis of actuator technologies for robotics. In: Khatib O, Craig JJ, Lozano-Perez T, editors. The robotics review 2. Cambridge, MA: MIT Press, 1991. p. 299–342.
[4] Grodski JJ, Immega GB. Myoelectric control on a ROMAC protoarm. Int Sym On Teleoperation and Control 1988:297–308.
[5] Schulte RA. The characteristics of the McKibben artificial muscle. In: the application of external power in prosthetics and orthotics. Publ. 874, Nas-Rc, 1962. p. 94–115.
[6] Daerden F, Lefeber D, Kool P. Using free-radical expansion pneumatic artificial muscles to control a 1 dof robot arm. In: CLAWAR Brussels '98 26–28 November, 1998. p. 209–14.
[7] Takahashi S. Piezo-electric actuators and their applications. J Inst Elect lnf Comm Engng 1987;70:295–7.
[8] Hayashi I, Iwatsuki N, Kawai M, Shibata J, Kitagawa T. Development of piezo-electric cycloid motorIEE Colloquium, London, No. 1991/146, 1991.
[9] Dario P, Bergamasco M, Bernardi L, Bicchi A. A shape memory alloy actuating module for fine manipulation. In: IEEE Micro-robots and Teleoperators Workshop, Hyannis, MA, 9–11 November, 1987.
[10] Pfieffer C, DeLaurentis K, Mavroidis C. Shape memory alloy actuated robot prosthesis: initial experiments. In: IEEE Robotics and Automation Conference, Detroit, USA, 1999. p. 2385–90.
[11] Scott D. Electro-Rheological (ER) fluid near commercial stage. Automotive Engng 1985;93:75–9.
[12] Caldwell DG. Compliant polymeric actuators as robotic drive units. Ph.D thesis, Department of Electronic Engineering, University of Hull, Hull, UK, 1990.
[13] Kuhn W. Reversible Dehnung und Kontraktion bei Anderung der Ionisation eines Netwerks polyvalenter Fadenmolekulionen. Expenmeuflo 1949;5:318–9.
[14] Katchalsky A. Rapid swelling and deswelling of reversible gels of polymeric acids by ionization. Experimentia 1949;5:319–20.
[15] Katchalsy A, Lifson S, Michaeli I, Zwick M. Elementary mechano-chemical process. In: Wassermann A, editor. Size and shape changes of contractile polymers. London: Pergamon Press, 1960.
[16] Osada Y, Hasebe M. Electrically activated mechano-chemical devices using polyelectrolyte gels. Chem Lett 1985:1285–8.
[17] Kornbluh R, Pelrine R, Eckerle J, Joseph J. Electrostrictive Polymer Artificial Muscle Actuators. In: IEEE Robotics and Automation Conference, Leuven, Belgium, USA, 1998. p. 2147–52.
[18] Flory PJ. Principles of polymer chemistry. New York: Cornell University Press, 1957.
[19] Tatara Y. Mechanical behaviour of mechanochemical materials: part 2, mechanical outputs in an equilibrium state. Bull JSME 1972;15:58–72.
[20] Wilkie DR. Muscle. London: Edward Arnold, 1976.
[21] Caldwell DG, Taylor PM. An artificial muscle actuator for robots. In: Waldron KJ, editor. Advanced robotics. Berlin: Springer-Verlag, 1989. p. 244–58.
[22] Caldwell DG, Medrano-Cerda GA, Goodwin MJ. Control of pneumatic muscle actuators. IEEE Control Systems Journal 1995;15:40–8.
[23] Chou P, Hannaford B. Static and dynamic characteristics of McKibben pneumatic artificial muscles. In: IEEE Conference on Robotics and Automation, San Diego, USA, May, 1994.

[24] Caldwell DG, Tsagarakis N, Medrano-Cerda GA, Schofield J, Brown S. Development of a pneumatic muscle actuator driven manipulator rig for nuclear waste retrieval operations. In: IEEE Robotics and Automation Conference, Detroit, USA, 1999. p. 525–30.
[25] Tsagakaris N, Caldwell DG. Performance modelling for pneumatic Muscle Actuators, Int Journal of Systems Science (to be published), 1999.